REPORT DOCUMENTATION PAGE

Form Approved OMB NO. 0704-0188

1. REPORT DATE (DD-MM-YYYY)	2. REPORT TYPE	3. DATES COVERED (From - To)
29-09-2014	Final Report	10-Aug-2010 - 9-Apr-2014

4. TITLE AND SUBTITLE
Final Report: Depth-Dependent Defect Studies Using Coherent Acoustic Phonons

5a. CONTRACT NUMBER
W911NF-10-1-0363

5b. GRANT NUMBER

5c. PROGRAM ELEMENT NUMBER
611102

6. AUTHORS
Stephanie Gilbert Corder, Norman Tolk

5d. PROJECT NUMBER

5e. TASK NUMBER

5f. WORK UNIT NUMBER

7. PERFORMING ORGANIZATION NAMES AND ADDRESSES
Vanderbilt University
PMB # 407749
2301 Vanderbilt Place
Nashville, TN 37240 -7749

8. PERFORMING ORGANIZATION REPORT NUMBER

9. SPONSORING/MONITORING AGENCY NAME(S) AND ADDRESS (ES)
U.S. Army Research Office
P.O. Box 12211
Research Triangle Park, NC 27709-2211

10. SPONSOR/MONITOR'S ACRONYM(S)
ARO

11. SPONSOR/MONITOR'S REPORT NUMBER(S)
56101-MS.12

12. DISTRIBUTION AVAILIBILITY STATEMENT
Approved for Public Release; Distribution Unlimited

13. SUPPLEMENTARY NOTES
The views, opinions and/or findings contained in this report are those of the author(s) and should not contrued as an official Department of the Army position, policy or decision, unless so designated by other documentation.

14. ABSTRACT
Presented is our scientific progress in two areas of research. The first is coherent acoustic phonon (CAP) spectroscopy of diamond crystals. We showed an ion implantation process significantly modifies the acousto-optical structure of diamond, resulting in a variety of features in the observed CAP spectra. These features were examined as a function of implantation dose and an empirical model was applied to the data, yielding good agreement. We continue this work by exploring the effects of single layer graphene on diamond with the goal of understanding how the relaxation dynamics of graphene is altered by coupling to different diamond interfaces and

15. SUBJECT TERMS
coherent acoustic phonons, diamond, silicon, photelastic coefficients, refractive index, graphene, Second Harmonic Generation

16. SECURITY CLASSIFICATION OF:			17. LIMITATION OF ABSTRACT	15. NUMBER OF PAGES	19a. NAME OF RESPONSIBLE PERSON
a. REPORT	b. ABSTRACT	c. THIS PAGE			Norman Tolk
UU	UU	UU	UU		19b. TELEPHONE NUMBER 615-322-2786

Report Title

Final Report: Depth-Dependent Defect Studies Using Coherent Acoustic Phonons

ABSTRACT

Presented is our scientific progress in two areas of research. The first is coherent acoustic phonon (CAP) spectroscopy of diamond crystals. We showed an ion implantation process significantly modifies the acousto-optical structure of diamond, resulting in a variety of features in the observed CAP spectra. These features were examined as a function of implantation dose and an empirical model was applied to the data, yielding good agreement. We continue this work by exploring the effects of single layer graphene on diamond with the goal of understanding how the relaxation dynamics of graphene is altered by coupling to different diamond interfaces and the effect of diamond on the scattering mechanisms involved and determining the efficiency of different pathways for energy relaxation. The second area of focus is a project assessing the transient strain produced by CAP waves. We have compared the measured CAP spectra to ab initio calculations of the opto-electronic properties of materials. We are also using CAP waves as an active moving interface to induce local changes in electric, acoustic, and optical properties. This is able to generate ultrafast, homogenous, transient localized strains of similar magnitude of other methods, thereby enhancing electronic and optical response of any target material.

Enter List of papers submitted or published that acknowledge ARO support from the start of the project to the date of this printing. List the papers, including journal references, in the following categories:

(a) Papers published in peer-reviewed journals (N/A for none)

Received		Paper
08/31/2012	3.00	Travis C. Wade, Dorothy W. Coffey, Nikkon Ghosh, James E. Wittig, Weng P. Kang, Lawrence F. Allard, Kinga A. Unocic, Jimmy L. Davidson, Norman H. Tolk. Nanostructure TEM analysis of diamond cold cathode field emitters, Diamond and Related Materials, (02 2012): 29. doi: 10.1016/j.diamond.2011.11.007
09/16/2013	5.00	Justin Gregory, Andrew Steigerwald, Hiroaki Takahashi, Anthony Hmelo, Norman Tolk. Erratum: “Ion implantation induced modification of optical properties in single-crystal diamond studied by coherent acoustic phonon spectroscopy” [Appl. Phys. Lett. 101, 181904 (2012)], Applied Physics Letters, (07 2013): 49904. doi: 10.1063/1.4816967
09/16/2013	6.00	H. Park, B. Choi, A. Steigerwald, K. Varga, N. Tolk. Annealing effect in boron-induced interface charge traps in Si/SiO2 systems, Journal of Applied Physics, (01 2013): 23711. doi: 10.1063/1.4773527
09/16/2013	7.00	W. F. Paxton, A. Steigerwald, M. Howell, N. Tolk, W. P. Kang, J. L. Davidson. The effect of hydrogen desorption kinetics on thermionic emission from polycrystalline chemical vapor deposited diamond, Applied Physics Letters, (12 2012): 243509. doi: 10.1063/1.4772069
09/16/2013	8.00	Justin Gregory, Andrew Steigerwald, Hiroaki Takahashi, Anthony Hmelo, Norman Tolk. Ion implantation induced modification of optical properties in single-crystal diamond studied by coherent acoustic phonon spectroscopy, Applied Physics Letters, (11 2012): 181904. doi: 10.1063/1.4765647
09/29/2014	10.00	H M Lawler, A Steigerwald, J Gregory, H Krzyzanowska, N H Tolk. Experimental and theoretical determination of the opto-acoustic spectrum of silicon, Materials Research Express, (04 2014): 0. doi: 10.1088/2053-1591/1/2/025701
TOTAL:		**6**

Number of Papers published in peer-reviewed journals:

(b) Papers published in non-peer-reviewed journals (N/A for none)

Received Paper

TOTAL:

Number of Papers published in non peer-reviewed journals:

(c) Presentations

"Ultrafast Relaxation Dynamics of Hot carriers and Phonons in Graphene-Diamond Interface", Zeynab Jarrahi. Poster presented at the Southeastern Section of the American Physical Society. Bowling Green, KY November 20-23, 2013
"Ultrafast Relaxation Dynamics of Hot carriers and Phonons in Graphene-Diamond Interface", Zeynab Jarrahi. Poster presented at the New Diamond and Nano Carbons Conference Chicago, Il. May 25-29, 2014
"Strain-induced SHG from Traveling Coherent Acoustic Phonons", Joy Garnett.
Poster presented at the Southeastern Section of the American Physics Society. Bowling Green, KY November 20-23, 2013

"Strain-induced second harmonic generation arising from a traveling coherent acoustic phonon pulse measured as a function of depth", Joy Garnett. Poster presented at the Gordon Research Conference on Thin Film and Small Scale Mechanical Behavior in Waltham, MA. July 12-18, 2014

"Dynamic second harmonic generation from SiO2/Si interfaces under temporally and spatially localized strain induced by coherent acoustic phonons", Halina Krzyzanowska. Materials Research Society Fall Meeting, Boston MA December 1-6, 2013

"Optical characterization of ion implantation defects in diamond using coherent acoustic phonon interferometry", Justin Gregory. Poster presented at Optics of surfaces and Interfaces 10, Chemnitz, Germany. September 8-13, 2013
"Optical characterization of ion implantation defects in diamond using coherent acoustic phonon interferometry" Justin Gregory. Poster presented at the International Conference on Diamond and Carbon Materials 2013, Riva del Garda, Italy. September 2013
"Probing depth-dependent defect concentrations and defect induced optoelectronic structure modifications in diamond with picosecond coherent acoustic phonon waves," N. Tolk, International Conference on Diamond and Carbon Materials, 2-5 September 2013, Riva del Garda, Italy

"Coherent Acoustic Phonon Waves: A Unique Approach To Perform Depth-Dependent Surface Physics In Bulk Materials" N. Tolk, 10th International Conference on Optics of Surfaces and Interfaces (OSI 10) Chemnitz, Germany, September 8th - 13th 2013.

Number of Presentations: 9.00

Non Peer-Reviewed Conference Proceeding publications (other than abstracts):

Received Paper

TOTAL:

Number of Non Peer-Reviewed Conference Proceeding publications (other than abstracts):

Peer-Reviewed Conference Proceeding publications (other than abstracts):

Received	Paper	
08/30/2011	1.00	Andrew Steigerwald, Justin Gregory, Kalman Varga, Anthony Hmelo, Xinyu Liu, Jacek Furdyna, Leonard Feldman, Norman Tolk. Study of depth-dependent radiation-induced defects using coherent acoustic phonon spectroscopy, 2011 MRS Spring Meeting. 26-APR-11, . : ,
TOTAL:	**1**	

Number of Peer-Reviewed Conference Proceeding publications (other than abstracts):

(d) Manuscripts

Received	Paper
TOTAL:	

Number of Manuscripts:

Books

Received	Book
TOTAL:	

Received	Book Chapter

TOTAL:

Patents Submitted

"A novel method for measuring order/disorder (defects, strain and impurities) in a material as a function of depth using depth-dependent second harmonic generation (SHG)"

Patents Awarded

Awards

Graduate Students

NAME	PERCENT_SUPPORTED	Discipline
Joy Garnett	0.06	
Stephanie Gilbert	0.07	
Zeynab Jarrahi	0.10	
FTE Equivalent:	**0.23**	
Total Number:	**3**	

Names of Post Doctorates

NAME	PERCENT_SUPPORTED
Halina Krzyzanowska	0.05
Justin Gregory	0.16
FTE Equivalent:	**0.21**
Total Number:	**2**

Names of Faculty Supported

NAME	PERCENT_SUPPORTED	National Academy Member
Norman Tolk	0.08	
FTE Equivalent:	**0.08**	
Total Number:	**1**	

Names of Under Graduate students supported

NAME	PERCENT_SUPPORTED
FTE Equivalent:	
Total Number:	

Student Metrics

This section only applies to graduating undergraduates supported by this agreement in this reporting period

The number of undergraduates funded by this agreement who graduated during this period:	0.00
The number of undergraduates funded by this agreement who graduated during this period with a degree in science, mathematics, engineering, or technology fields:.....	0.00
The number of undergraduates funded by your agreement who graduated during this period and will continue to pursue a graduate or Ph.D. degree in science, mathematics, engineering, or technology fields:.....	0.00
Number of graduating undergraduates who achieved a 3.5 GPA to 4.0 (4.0 max scale):.....	0.00
Number of graduating undergraduates funded by a DoD funded Center of Excellence grant for Education, Research and Engineering:.....	0.00
The number of undergraduates funded by your agreement who graduated during this period and intend to work for the Department of Defense	0.00
The number of undergraduates funded by your agreement who graduated during this period and will receive scholarships or fellowships for further studies in science, mathematics, engineering or technology fields:	0.00

Names of Personnel receiving masters degrees

NAME
Total Number:

Names of personnel receiving PHDs

NAME	
Justin Gregory	
Total Number:	**1**

Names of other research staff

NAME	PERCENT_SUPPORTED
FTE Equivalent:	
Total Number:	

Sub Contractors (DD882)

Inventions (DD882)

5 **Invention disclosure "A novel method for measuring order/disorder (defects, strain and impurities) in a material as a funct**

Patent Filed in US? (5d-1) Y

Patent Filed in Foreign Countries? (5d-2) N

Was the assignment forwarded to the contracting officer? (5e) N

Foreign Countries of application (5g-2): We intend to file in Foriegn Countries

5a: Halina Krzyzanowska

5f-1a: Vanderbilt University

5f-c: VU Station B #351807

Nashville TN 37235

5a: Norman Tolk

5f-1a: Vanderbilt University

5f-c: VU Station B #351807

Nashville TN 37235

5a: Joy Garnett

5f-1a: Vanderbilt University

5f-c: VU Station B #351807

Nashville TN 37235

Scientific Progress

Technology Transfer

Final Report:

Depth-Dependent Defect Studies Using Coherent Acoustic Phonons

Table of Contents

List of Figures

Abstract

Presented is our scientific progress in two areas of research. The first is coherent acoustic phonon (CAP) spectroscopy of diamond crystals. We showed an ion implantation process significantly modifies the acousto-optical structure of diamond, resulting in a variety of features in the observed CAP spectra. These features were examined as a function of implantation dose and an empirical model was applied to the data, yielding good agreement. We continue this work by exploring the effects of single layer graphene on diamond with the goal of understanding how the relaxation dynamics of graphene is altered by coupling to different diamond interfaces and the effect of diamond on the scattering mechanisms involved and determining the efficiency of different pathways for energy relaxation. The second area of focus is a project assessing the transient strain produced by CAP waves. We have compared the measured CAP spectra to ab initio calculations of the opto-electronic properties of materials. We are also using CAP waves as an active moving interface to induce local changes in electric, acoustic, and optical properties. This is able to generate ultrafast, homogenous, transient localized strains of similar magnitude of other methods, thereby enhancing electronic and optical response of any target material.

Spatial extent of optical modification due to lattice disorder in GaAs

We have measured ion beam-induced optoelectronic modifications in GaAs as a function of depth using CAP spectroscopy. The basic effect is well explained by defect-modified changes in the electronic properties near the semiconducting band edge. A simple geometric model of the dose dependence suggests that band-gap modification may be characterized by a defect induced strain field that sweeps out a volume almost 10 nm in diameter, modifying the electronic structure at hundreds of nearby lattice points. While this effect is quite long-range for energies very near the band edge it reduces dramatically as the energy is detuned from E_g. Our results suggest that optical modification surrounding the amorphous state extends well beyond the structural disorder, suggesting a fundamental upper limit for the achievable density of bits/cm^2 in optical applications. These examples serve to highlight the importance of the relationship between structural and optoelectronic disorder in a wide variety of applications.

Sets of 1 cm^2 [100] GaAs wafers were implanted with 400keV Ne^{++} ions at doses between 10^9–10^{15} ions/cm^2. Samples were then cleaved, and one piece from each sample was deposited with 10nm Al to act as an absorbing layer in the CAP experiment. The depth-dependent point defect concentrations have a roughly Gaussian profile peaking at about z = 450 nm, as determined by our simulations. CAP measurements were performed in a standard time-resolved pump-probe setup in reflection geometry using a Coherent 76MHz laser [1,2]. Sample pieces not deposited with Al were used for ion beam channeling analysis performed using 1.8 MeV He^+ ions generated from a 2.0 MeV electrostatic Van de Graaf accelerator. Samples used for CAP measurements and channeling analysis were kept separate. In addition to channeling analysis, we also carried out Monte Carlo simulations using the Transport of Ions in Matter (TRIM) code [3], which allows us, in principle, to estimate the structural damage at doses below the sensitivity of the channeling technique.

The total pump-probe response for an undamaged and damaged sample is shown in Figure 1(b). Unless otherwise noted, $E_{probe} = 1.41$ eV, the experimentally determined GaAs band gap. In the damaged sample the CAP amplitude is reduced at early time delays, where radiation damage is expected. The isolated oscillatory responses for selected doses are shown in Figure 1(c), superimposed on the undamaged response. The slow attenuation seen in all responses is due to the linear absorption of the probe light ($\alpha_{GaAs}(1.41\text{ eV}) \approx 10^2\text{ cm}^{-1}$).

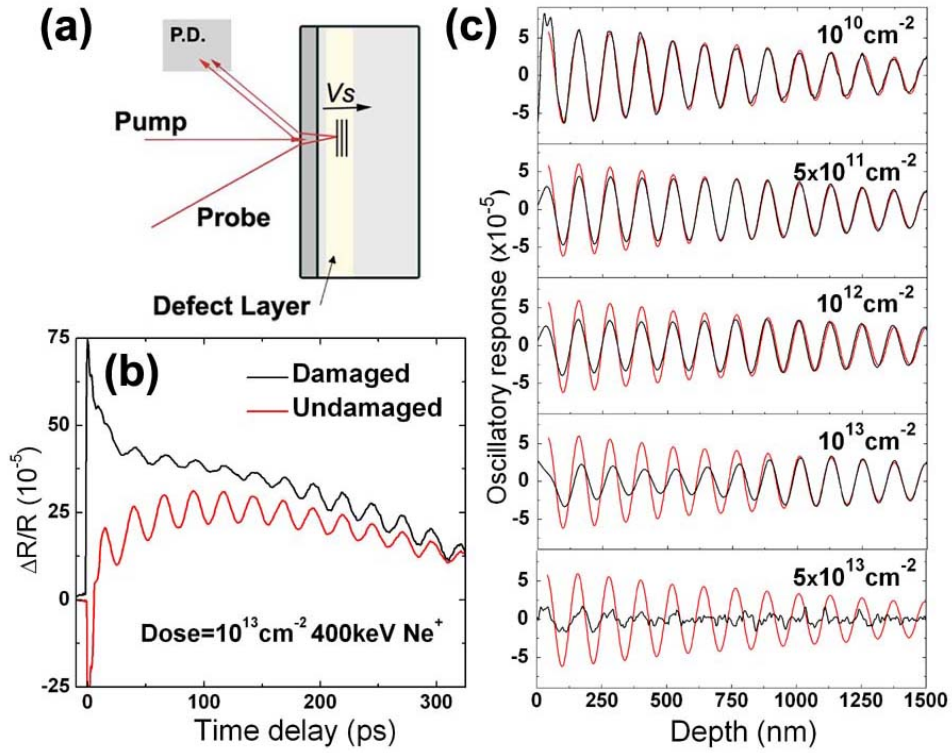

Figure 1: (a) A cartoon schematic showing the generation and detection of the acoustic wave. (b) The total pump-probe differential reflectivity response for an as-grown sample and a sample exposed to 10^{13} Ne^{++} ions/cm^2. (c) Isolated oscillatory responses for samples exposed to various irradiation doses superimposed on the undamaged response.

Samples below 10^{11} cm^{-2} show no noticeable change in the oscillation pattern, while above 5×10^{13} cm^{-2} the CAP signal is quickly damped. Between 10^{11} and 10^{13} cm^{-2}, distinct amplitude modulation is observed for depths less than 1 μm below the surface, after which both signals become equal in period and amplitude. This observation of the long-time (deep depth) similarity between damaged and undamaged signals is important to our analysis. At the disorder peak we expect many changes to material properties, including the elastic constants and index of refraction. However, a significant deviation of any of these values in the near-surface damage region should modify the *long-term* (i.e. long time delay) behavior of the optical response, either through a phase change or amplitude attenuation. As we observe no difference between the long-term behavior of undamaged and damaged samples below 5×10^{13} cm^{-2}, we conclude that while in

principle these properties are modified in the damaged regions, they are below our experimental sensitivity. However, it is possible for the photoelastic constants to differ significantly, and we conclude that changes to $dn/d\eta$ and $d\kappa/d\eta$ are responsible for the observed amplitude reduction.

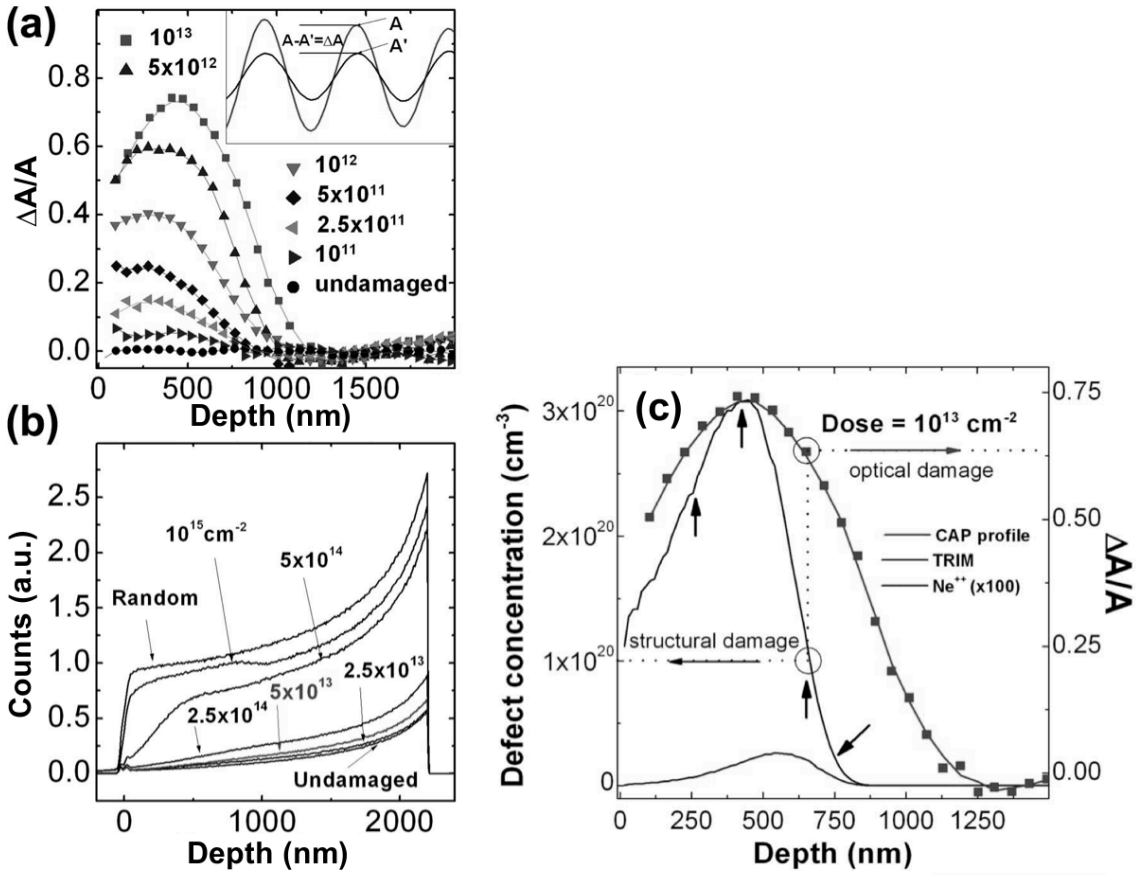

Figure 2: (a) CAP profiles for doses between 10^{11} and 10^{13} Ne^{++} ions/cm^2. Inset: definition of ΔA/A. (b) Channeling spectra for doses between 2.5×10^{13} and 10^{15} Ne^{++} ions/cm^2. (c) Comparison between CAP and TRIM profiles demonstrating how ΔA/A values are paired with estimated defect concentrations (n_d) (see dotted lines).

The $dn/d\eta$ and $d\kappa/d\eta$ terms may be rewritten as:

$$\frac{d[n,\kappa]}{d\eta} = \frac{d[n,\kappa]}{dE^*}\frac{dE_g}{d\eta}$$

where E^* is defined as $E_g - E_{probe}$. The first factor represents the change in the optical constants for energies around the band gap (E_g), while $dE_g/d\eta$ is the deformation potential ($dE_{probe}/d\eta$ is zero by definition). Assuming $dE_g/d\eta$ is constant, the observed changes must be due to a reduction of the first term. In fact, this is the well-known band tailing phenomenon, first studied in impure semiconducting crystals displaying energy "tails" extending into the band gap [4]. This broadens the band edge and results in reduced

derivative values, observed experimentally as reduced CAP amplitude. In this context, the local disruption of electron densities in areas of high disorder is the microscopic analog of the macroscopic observation of band tailing.

CAP spatial profiles (Figure 2(a)) are constructed by defining $\Delta A = A - A'$, where A and A' are the values of the undamaged and damaged oscillation peaks, respectively. ΔA is then divided by A to account for linear absorption of the probe light, yielding only changes caused by the irradiation process (see Figure 2(a), inset). Figure 2(b) also shows ion channeling spectra for selected samples [5,6]. The energy spectra are well understood and indicate the level of structural damage caused by the ion bombardment at relatively high doses. The minimum sensitivity of the channeling technique was observed to be near 5×10^{13} cm^{-2} (~1% atomic displacement), roughly equal to the *upper* limit of the optical technique. Defect profiles were obtained from the data in Figure 2(b) following the multiple scattering method of Ref. 41. Figure 2(c) shows that the optical modification of the GaAs extends well beyond the structural damage. Thus, we conclude that TRIM simulations provide a good measure of structural damage as verified by channeling analysis, as well as opto-electronic modifications as verified by CAP, which can be extended to doses well below the sensitivity of the channeling technique.

Studies of ion-beam induced damage in diamond lattices

Reliable fabrication of single-photon emitting centers and photonic devices in diamond using ion implantation techniques will require a detailed understanding of the associated defects created within the lattice during the implantation process, and how those defects modify the optical properties of diamond. Despite decades of work [7,8] on ion implantation in diamond and the optical properties of diamond defects, many questions remain concerning the specific relationships between the structural modifications of the diamond lattice and the resulting modulation of local optical properties. In this study, we have applied CAP interferometry to characterize the depth-varying modulation to the optical characteristics of ion-implanted diamond crystals. Since the band gap of diamond (~5 eV) is much larger than that of GaAs (~1.5 eV), our optical probe at 400 nm (3 eV) accesses mid-gap states. This leads to very different behavior in the observed CAP spectra as compared to the GaAs studies described above.

Experimental details

Single-crystal (100) CVD diamond samples were purchased from the Element Six Corporation. A Van de Graaff accelerator was used to implant the samples with 1.0–1.5 MeV He^+ ions, with doses ranging from 10^{14} to 10^{17} cm^{-2}. Implantations were performed in vacuum below zero degrees Celsius. Implanted samples were coated with 10 nm of Al using electron beam and resistive evaporation. Optical pump-probe CAP measurements were taken using a Coherent Mira 900 Ti:Sapphire laser producing 150-fs pulses at 76 MHz. The pump beam was tuned to 800 nm with an average power of 150 mW, and the probe beam was frequency-doubled to 400 nm with a typical average power of 2.1 mW. Both beams were focused on the sample with a typical spot diameter of 100 μm for the pump and 50 μm for the probe. To reduce noise, the pump beam was modulated at 50 kHz using an acousto-optical modulator and the probe beam was monitored using a lock-in amplifier.

To model the lattice damage resulting from ion implantation, Monte Carlo simulations were performed using the Stopping and Range of Ions in Matter (TRIM). The model parameters were 3.515 g/cm^3 for the density and 52 eV for the displacement energy.

Results and Discussion

Figure 3 shows CAP oscillations at several doses for the implanted diamond specimens. There are three key features of the oscillations. The first and most striking is the appearance of a 'pulse', which increases in size and has an earlier onset with increasing dose. Although the implanted and unimplanted oscillations before and after the pulse feature are essentially in phase, the oscillations in the pulse feature are directly out-of-phase with the unimplanted oscillations.

In addition to the pulse feature, it may be observed that there is a small phase shift in the region beyond the implantation damage, which increases with increasing dose. The third and final feature is the amplitude loss in the oscillations, which is persistent beyond the damaged region, and increases with implantation dose.

Figure 4 shows aspects of each of the three features described above as a function of implantation dose. These features are due to a variety of opto-electronic interactions between the damaged lattice and the optical probe. The pulse feature may be explained by taking into account the damage-induced modulation of the photoelastic coefficient $dN/d\eta$ of diamond. Ordinarily, this coefficient is positive in diamond at 400 nm. The travelling strain wave in the CAP experiment therefore creates a traveling optical interface with an increasing real index of refraction; this results in a 180° phase shift in the reflected electromagnetic wave. As the implantation damage is increased, the photoelastic coefficient decreases, which decreases the reflectivity of the traveling strain wave. At the critical damage level of 3.9×10^{20} cm^{-3}, the coefficient becomes zero, and there is no reflectivity. At this point no CAP oscillations are visible. This is the node at the onset of the pulse feature. As the vacancy concentration increases beyond the critical level, the photoelastic coefficient becomes negative. Now the strain wave generates an optical interface with *decreased* index, reversing the interference effect at the sample surface since there is no phase shift in the reflected light.

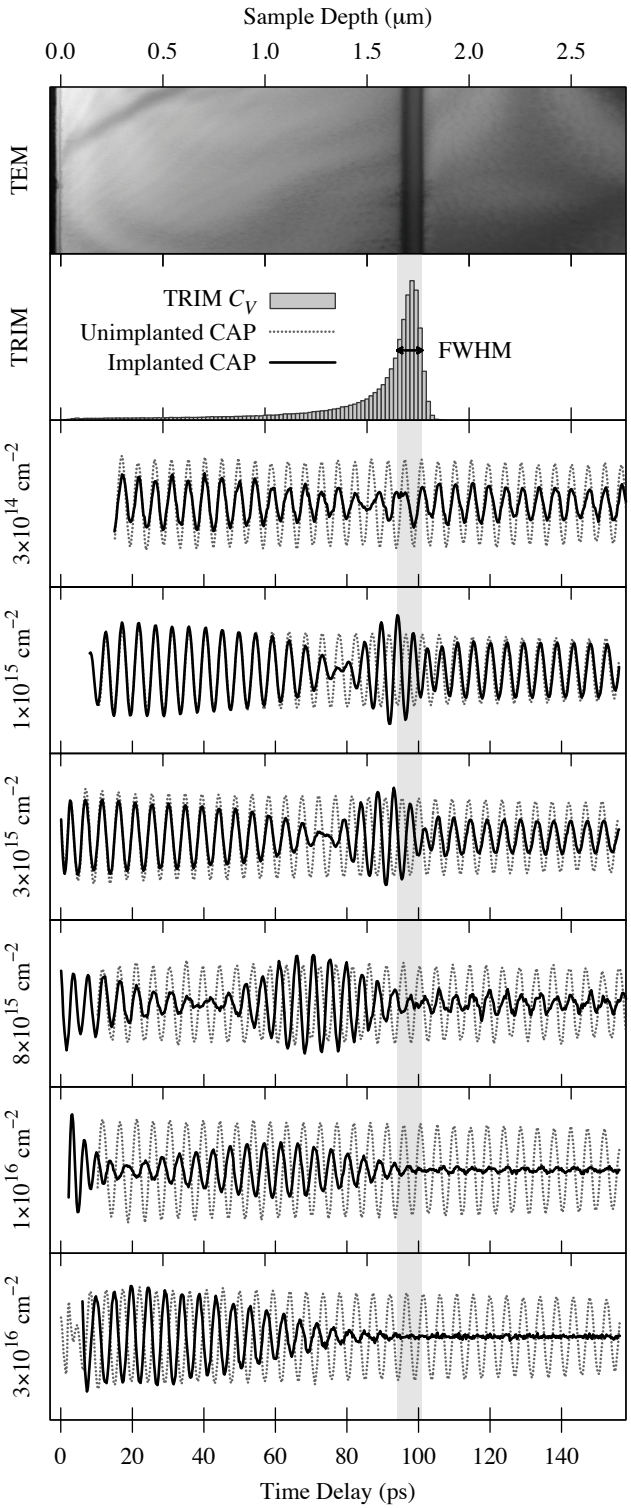

Figure 3: CAP oscillations in implanted diamond specimens (black lines) at various doses. The corresponding unimplanted oscillations are shown as dotted lines. The top frame shows a cross-sectional TEM image for the $3x10^{16}$ cm^{-2} fluence. The second frame shows the implantation-induced vacancy concentration profile as calculated by TRIM. The vertical bar is the FWHM of the TRIM calculation.

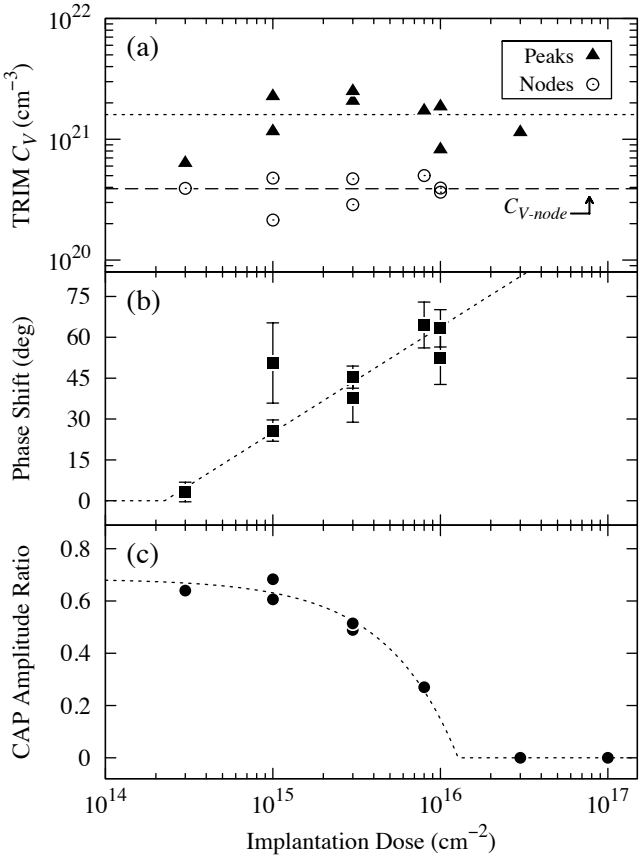

Figure 4: Oscillation features versus implantation dose. (a) TRIM vacancy concentrations for the peak of the pulse feature and the node at its onset ($C_{V\text{-}node}$ = 3.9×10^{20} cm^{-3}). (b) Phase shift in the region beyond the implantation damage. (c) Oscillation amplitude ratio between the region beyond the implantation damage and the region near the sample surface.

The gradual phase shift in the oscillations beyond the damaged region is attributed to a damage-induced decrease in the real refractive index of the specimens in the implanted zone. This decreases the optical path length of the traveling probe pulse. There has been some controversy [9-16] concerning the variation of diamond's refractive index due to implantation damage. Usually, ion implantation decreases the refractive index of materials, due to the associated decrease in material density via the introduction of vacancies. However, in diamond, this effect is in competition with the dramatic change in polarizability brought on by the reconfiguration of sp^3 and sp^2 bonds. It seems that in diamond, this effect may overpowers the decrease in density, thus the net effect in some studies is an increase in the real refractive index.

The amplitude loss is shown in Figure 4(c), along with a linear fit of the data. This feature is attributed to the damage-induced increase in the absorption of the specimen, specifically the imaginary part of the refractive index. This observation is confirmed by naked-eye observation: the implanted regions of the specimens grow visibly darker with increasing dose, and are fully opaque at the highest doses.

Simulation and Quantitative Model

It is highly desirable for diamond-based optical device design perspective to develop a predictive, quantitative model to describe the variation in the optical characteristics of the diamond lattice due to ion implantation. To this end, the time-domain reflectivity of the implanted specimens is calculated using a numerical approach that employs the multiplication of homogeneous characteristic matrices for a series of discreet layers, each with a unique value of the complex index N as determined by the following equation:

$$N(z,t) = N\big(C_V(z)\big) - \tfrac{1}{2}\Big[N\big(C_V(z)\big)\Big]^3 p_{12}\big(C_V(z)\big)\eta(z,t).$$

Here C_V is the local vacancy concentration in the diamond lattice, which is determined for each implantation fluence using the TRIM code. N and p_{12} are now analytical functions of C_V. Excellent agreement between simulation and experiment are found by employing the following model:

$$n(C_V) = 2.4542 - 0.0153\left(1 - \exp\left[-\frac{C_V}{3.418\times 10^{19}\ \mathrm{cm}^{-3}}\right]\right)$$

$$\kappa(C_V) = 0.0025 + 0.112\left(1 - \exp\left[-\frac{C_V}{2.229\times 10^{21}\ \mathrm{cm}^{-3}}\right]\right)$$

$$p_{12}(C_V) = 0.044 - 0.145\left(1 - \exp\left[-\frac{C_V}{1.177\times 10^{21}\ \mathrm{cm}^{-3}}\right]\right)$$

Here, each optical property (n, κ, p_{12}) has an initial unperturbed value, a saturation value at high vacancy concentrations, and a coefficient that determines the rate of saturation. The comparison between the model and experiment is shown in Figure 5.

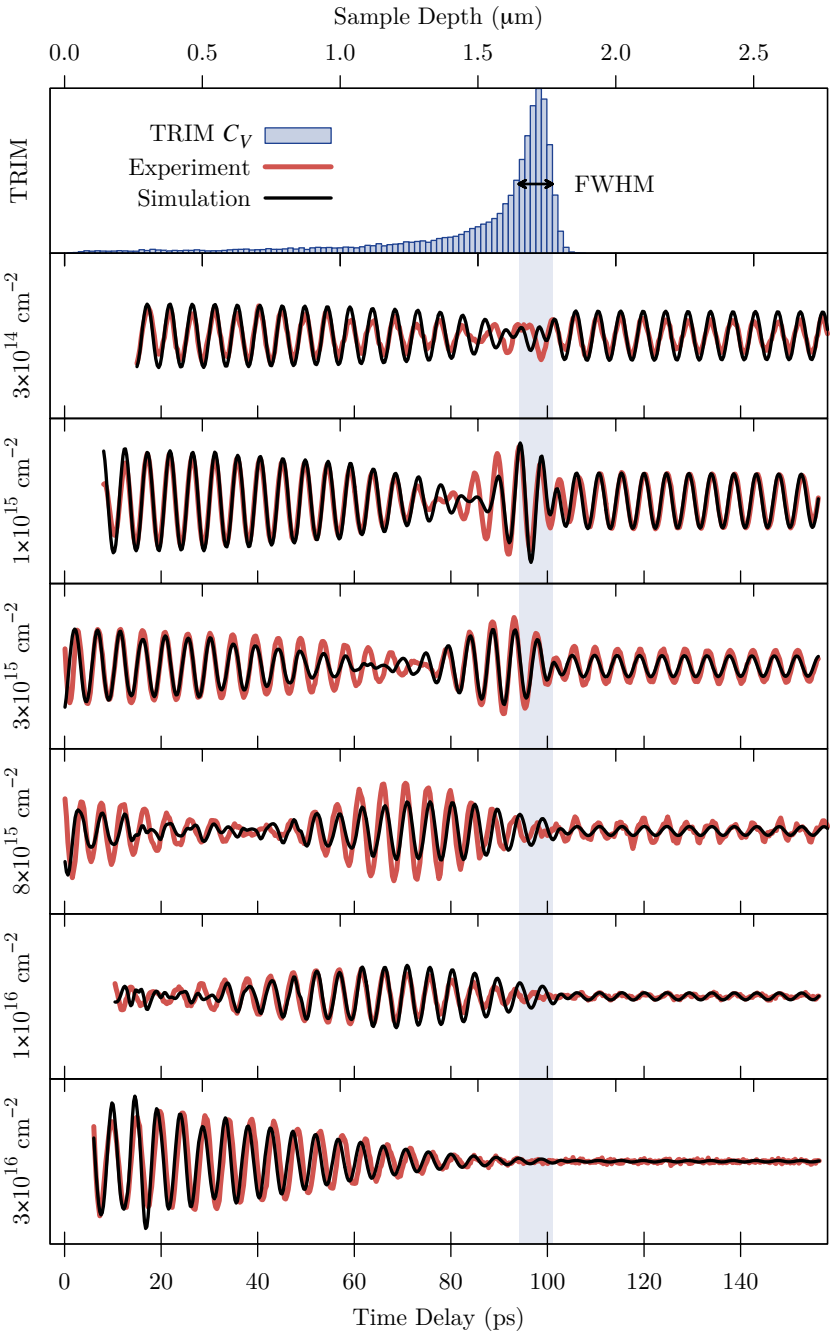

Figure 5: Comparison of the best fit of the exponential model (black) and experimental data (red) at the fluences studied.

Experimental Progress on Graphene on Diamond

In this project, we used femtosecond pump probe spectroscopy to contrast the population dynamics of photoexcited carriers and optical and acoustic phonons in single layer graphene transferred onto different diamond substrate. Graphene exhibits extremely high electron mobility and thermal conductivity. The ease of integrating graphene on almost

any substrate makes graphene an excellent candidate for advanced electronic applications. However, the presence of any substrate inevitably influences the electrical and thermal properties of graphene. Recently it has been shown that diamond might be close to the ideal substrate for graphene interconnects and field effect transistors. In this study we target the specific mechanisms of the electron and phonon relaxation processes at the graphene/diamond interface for further understanding the enhanced performance of graphene-diamond FETs.

Experiment

We transferred single layer CVD grown graphene on polycrystalline diamond and (100) face of single crystalline diamond as can be seen in the SEM images Figure 6. Raman spectroscopy ensures that we have high quality single layer graphene. We then proceeded to carrying out the pump probe spectroscopy measurements using a Ti-sapphire laser with a pulse duration of ~120 fs. The measured transient differential transmission spectra (shown in Figure 7) show a bleaching of the optical response due to the Pauli blocking and a fast recovery of transmission that can be analytically fit to biexponential decay. We attribute the fast decay dynamics to the intraband and interband scattering phenomena between the thermalized distribution of electrons and the optical phonons. The slower relaxation can be attributed to the cooling of the subsystem of hot optical phonons by optical-acoustic phonon scattering. We observe that at different pump energy and powers, the time scales associated with this relaxation are consistently much faster for the single crystal diamond compared to any other substrate that we measured which in turn translates into faster and more efficient energy removal from the interface. Understanding how the relaxation dynamics of graphene is altered by coupling to different diamond interfaces and the effect of diamond on the scattering mechanisms involved and determining the efficiency of different pathways for energy relaxation, will pave the way towards realization of high performance carbon sp^2/sp^3 technology.

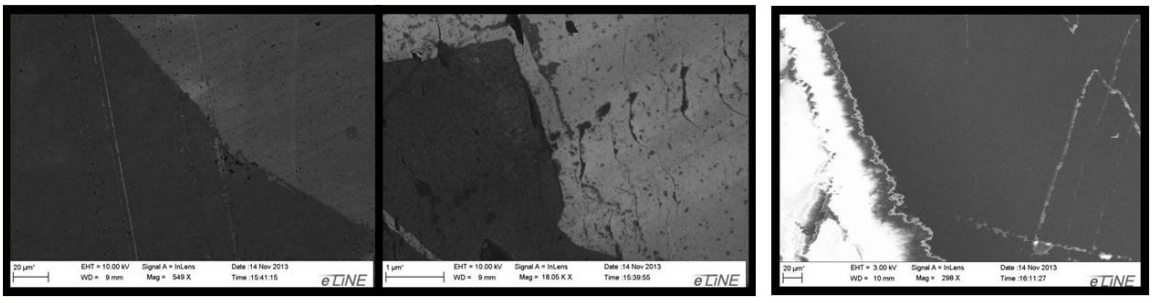

Figure 6: Left and Center: Graphene on single crystal diamond. Right: Graphene on poly-crystalline diamond.

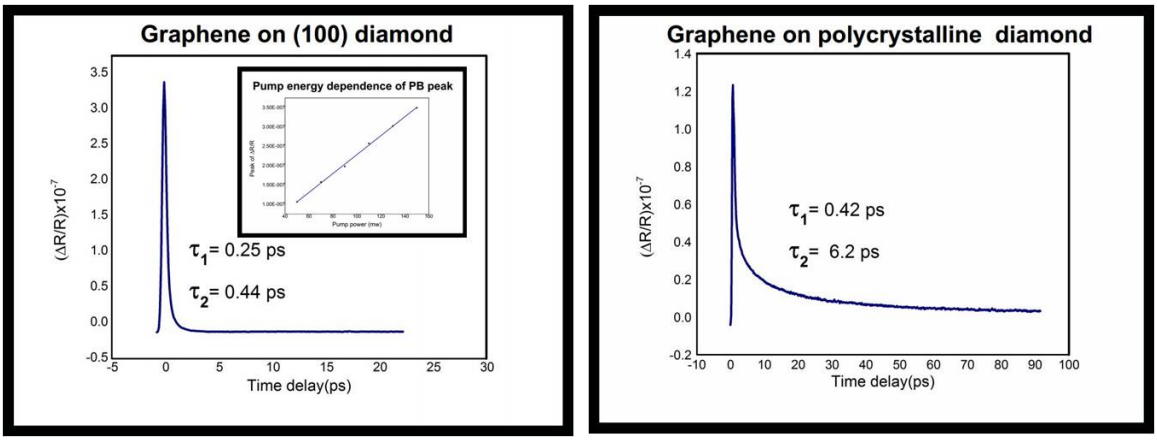

Figure 7: Left: Transient differential reflection spectra of graphene on (100) single crystal diamond. Right: Graphene on poly-crystalline diamond.

Experimental and theoretical determination of the opto-acoustic spectrum of silicon

One difficulty in analyzing the reflectivity response CAP experiments is that the reported photoelastic photon energy spectra for semiconducting materials are often inadequate. However, *ab initio* approaches using density functional theory allow one to calculate the photoelastic spectra and provide a predictive tool to guide experimental efforts. Here we report measurements and calculations for bulk Si(100) in the photon energy range 1.5–3.4 eV. The first-principles calculations of the photo-elastic spectra show remarkable agreement with measured CAP spectra. The results indicate that first-principles theoretical methods are feasible tools for interpretation of CAP spectra, and in the future will be used to characterize depth dependent defect concentrations.

Experiment

Si(100) wafers were sectioned with 10 nm layers of Al deposited. The film was deposited in vacuum at a pressure close to 10^{-6} Torr. The native oxide layer was not removed prior to deposition of the Al layer. The optical measurements were performed using a Coherent Ti:Sapphire 76MHz femtosecond pulsed laser setup in a time-resolved pump-probe reflectivity geometry. The pulse width was close to 150 fs and the bandwidth was about 7 nm. The pump and probe spot sizes were approximately 75 and 25 μm in diameter, respectively, and the pump fluence was held at 22 μJ/cm^2 for all measurements.

The CAP response of these samples was studied in two photon energy ranges, 1.4–1.8 eV, corresponding the tuning range of the laser, and 2.7–3.5 eV. For measurements in the low energy range the pump and probe photon energies were equal ($E_{probe} = E_{pump}$), while for the high-energy measurements the probe was passed through a doubling crystal before being directed onto the sample ($E_{probe} = 2E_{pump}$). Prior to each measurement the probe pulse reflectivity of the sample (R_0) was recorded, and the pump-probe data were divided by their respective R_0 values to obtain the normalized pump-induced change in the reflectivity, $\Delta R/R_0$.

Figure 8(c) shows selected isolated CAP responses of the Si(100) wafers from both the low and high-energy regions. Responses for 1.55 and 1.72 eV have been enhanced 10× for comparison with the higher energy responses. In addition to the spectra shown, data were collected at 1.47, 1.51, 1.59, 1.63, and 1.69 eV in the low energy region and 2.81, 2.95, 3.02, 3.26, 3.35, and 3.39 eV in the high energy region. Red solid lines in Figure 8(c) correspond to fits to the data.

Calculations

Generally, the photoelastic constants are expressed as a rank-four tensor connecting the strain and loss function tensors [17]. In diamond-type symmetry, notation is contracted. For small [001] uniaxial strains in Si, the dielectric constant varies approximately as,

$$-\left(\frac{1}{\varepsilon_b^2}\right)\delta\varepsilon_{ij} = \frac{\delta a}{a}\begin{pmatrix} p_{12} & 0 & 0 \\ 0 & p_{12} & 0 \\ 0 & 0 & p_{11} \end{pmatrix}$$

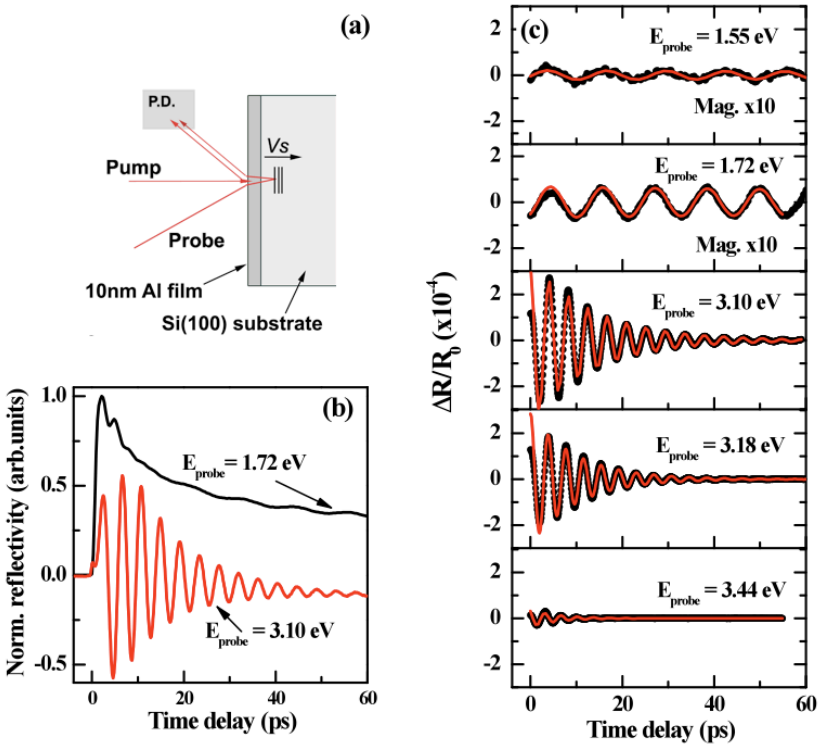

Figure 8: (a) Coherent acoustic phonon generation and detection scheme for Al(10nm)/Si(100) samples. (b) Full normalized time-resolved response for 1.72 eV (pump) / 1.72 eV (probe) and 1.55 eV (pump) / 3.10 eV (probe) measurements. (c) Sequence of isolated $\Delta R/R_0$ CAP responses for selected probe energies, with red lines as fits; CAP spectra at 1.55 eV and 1.72 eV have been magnified by a factor of 10 for visual comparison.

where ε_b is the bulk dielectric constant, the lattice constant is a, and $\delta a/a = \eta$ [18]. The laser probe field is transverse, so only the element p_{12} is relevant to the CAP measurements. All results are from finite difference calculations with strain of $\eta = \pm 0.5\%$, unless indicated otherwise. The spectra are calculated, including excitonic effects, with AI2NBSE [19], the ABINIT package [20], and Troullier-Martins pseudopotentials. The calculations implement 512 crystal-momenta points in the Brillouin zone. The local-density functional bandgap was corrected with a scissor shift of 0.6 eV. For photon frequency 0.35 eV, earlier calculations gave $p_{12} = 0.02$ (Ref. 17) and $p_{12} = 0.03$ (Ref. 18), and the value has been previously measured at $p_{12} = 0.02$ (Ref. 21). The value we calculate is slightly higher at $p_{12} = 0.04$.

Results and Discussion

Pump-probe data (Figure 8) were fit using a decaying sinusoid with amplitude A, and this parameter was extracted for each E_{probe}. Figure 3 shows the measured and calculated CAP amplitude. The plot from theory uses first-principles calculations of photo-elastic response and the sensitivity function F_1. The quantitative comparison between theory and experiment is made possible by inserting the calculated values of $dn/d\eta$, $dk/d\eta$ and n, k into Equations 2 and 4, respectively. Here A_0 was calculated to be 3.0×10^{-5} using the

values $\alpha_{pump} = 1.25\times10^{-6}$ cm^{-1}, $R_{pump} = 0.9$, $Q = 22$ μJ/cm^2, $\rho = 2.70$ g/cm^3, $v_s = 6420$ m/s, $B = 76$ GPa, $\beta = 23\times10^{-6}$ K^{-1}, and $C_v = 2.4$ J/cm^{3}K. A_0 was calculated assuming negligible absorption by the Si(100) substrate. Further, α_{pump} and R_{pump} vary by 2–3% each as the pump energy is tuned from 1.4–1.8 eV, and significant variation in elastic constants may exist between amorphous sputtered aluminum films and bulk literature values. We therefore consider a conservative estimate of the error in A_0 to be around 10%.

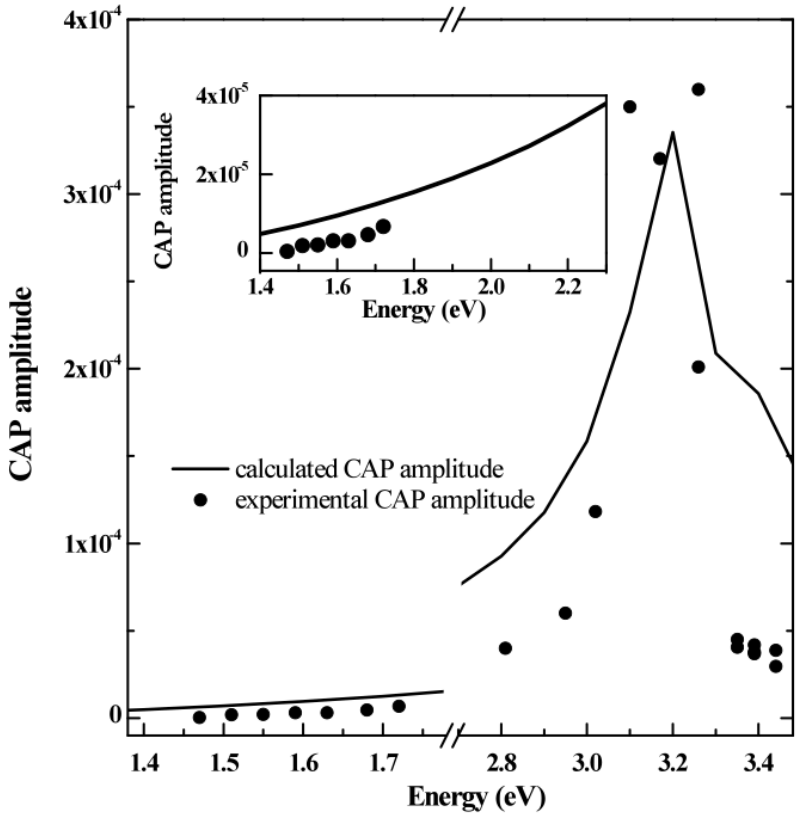

Figure 9: Comparison of theoretical (line) and experimental (dots) CAP amplitudes. The inset presents an expanded view of the 1.4–2.3 eV range for the experimental and theoretical CAP responses.

The inset of Figure 9 shows the low-energy CAP amplitude as measured and calculated. Both show CAP amplitudes less than 10^{-5} at 1.5 eV, comparable to our experimental sensitivity. Both experimental and theoretical amplitudes approximately double between 1.5 eV and 1.7 eV. This increase is related to dispersion in the real part of the photo-elastic constant. As a consequence, the signal becomes much easier to measure above 1.5 eV.

The measured and calculated amplitudes begin a rapid increase near 2.8 eV, as seen in Figure 9. This resonant response arises primarily from the photo-elastic effect, and is dominated by the imaginary part of the photo-elastic constant. The theoretical amplitude does not decrease as rapidly as the measured amplitude above 3.2 eV.

Conclusion

We have demonstrated excellent agreement between *ab initio* first-principles calculations and CAP spectroscopic measurements of the opto-acoustic response in Si(100) substrates. Our calculation is shown to be consistent with the measured reflectivity behavior across the entire studied energy range, including the experimental observation that the CAP response increases by two orders of magnitude from 1.5 eV to 3.2 eV, the latter of which is in the vicinity of the $E_{\Gamma 1}$ direct band edge of silicon. We were also able to reproduce the time-domain reflectivity CAP response observed experimentally with good agreement.

Accurately predicting the opto-acoustic response of a material like Si(100) allows one to utilize the full power of first-principles calculations and go beyond Maxwellian analytical or phenomenological models in order to model the PE response in defected or disorder materials. Our study motivates the extension to a theory-driven experimental study of dopant profiling, noninvasive nanometer-scale strain field analysis, and point-defect studies, among other applications.

Progress in Transient Strain-Induced Second Harmonic Generation Studies

Strain has been shown to enhance the optical and electronic performance of semiconductor based devices and thin film systems. Electronically, the energy band gap distorts due to strain-induced defects, thereby increasing electric mobility up to 70%. Optically, strain can introduce or enhance already existing second harmonic generation (SHG) up to 47% by destroying lattice centrosymmetry, increasing the second order optical nonlinear susceptibility , $X^{(2)}$.

Strain can be induced in semiconductor devices and thin films with several different passive and active techniques. Passively, strain can be induced by ion implantation or epitaxial fabrication techniques like molecular beam epitaxy (MBE). Actively, strain can be induced with external strain machines or with traditional acoustic excitation techniques. All of these strain methods have been shown to enhance second order optical nonlinear susceptibility $X^{(2)}$ and consequently second harmonic generation. However, these methods have limitations. With ion implantation and MBE methods alone, the strain is fixed, permanent and varies depending on which complicated fabrication protocols are employed.

Conventional active methods, like external strain machines and traditional acoustics provide a changeable, transient strain that can work with various materials, but also have some limitations as well. External strain machines produce an inhomogenous strain over a large area and cannot be incorporated directly into microelectronic or optoelectronic devices. Traditional acoustic waves produce homogenous strain and can be incorporated directly into devices. However, the speeds at which these acoustic frequencies can be generated are limited to low GHz, which makes them too slow for ultrafast processes. Frequencies obtainable with pump-induced acoustic waves are on the order of 10's of GHz to low THz. In our group, we induce strain via longitudinal coherent acoustic phonon (CAP) waves to reveal second harmonic generation (SHG) on an active moving

interface in semiconductors at room temperature with an ultrafast laser pump-probe technique. This technique produces an active strain interface, which induces local changes in electric, acoustic, and optical properties.

Second harmonic generation (SHG) is a nonlinear optical technique that has proven valuable for the characterization of the electronic characteristics of surfaces and interfaces. The inversion symmetry found in centro-symmetric materials precludes the observation of SHG signals in most crystals. However, the travelling strain pulse in a CAP experiment disrupts such symmetries, and thus provides a source for frequency-doubled photons. Our experimental approach is to combine CAP and SHG to study non-centrosymmetric materials such as polymer films, in much the same way as the Raman study discussed above. We are in the process of extending this approach to studies of heterostructured semiconductor systems with the end goal of providing a novel method for depth-sensitive symmetry related evaluation of complex materials systems.

The use of femtosecond laser pulses to characterize and control material properties at the quantum level has led to exciting developments at the frontier of condensed-matter physics. In this invention, we propose a novel method for using highly localized acoustic phonons to induce dynamic strain to improve performance. This novel depth-dependent characterization technique can accurately examine order/disorder effect (produced by defects, dopants, dynamic strain, etc.) versus depth. Due to direct measurement of second order non-linear susceptibility, we are able to extract elements of photoelastic and strain tensors under transient elastic strain and their respective effect on the material's electronic structure. This technique has a spatial resolution on the order of tens of nanometers, is noninvasive and nondestructive, has applicability primarily dependent on the transparency of the optical light, and is conducive to integration into fabrication processes. This technique will be particularly useful in thin film growth stages and inspect quality of structures used in optoelectronic industry, where lateral dimensions are on the order of microns, but depth dimensions are on the order of tens of nanometers.

We note that use of elastic strain has been shown to influence and in many cases enhance, the optical and electronic performance of semiconductor based devices [22,23]. Electronically, the imposition of strain has been measured to increase electric mobility by 70% [24]. Optically, the presence of strain modifies the tensor elements of the second order optical nonlinear susceptibility, $\chi^{(2)}$ leading to significant enhancement of the second-harmonic generation (SHG) response in a single crystal up to 47% by destroying lattice centrosymmetry, increasing the second order optical nonlinear susceptibility , $\chi^{(2)}$ [25].

Strain can be induced in semiconductor devices and thin films with several different passive and active techniques. Passively, strain can be induced by ion implantation or epitaxial fabrication techniques like molecular beam epitaxy (MBE). Actively, strain can be induced with external strain machines or with traditional acoustic excitation techniques. All of these strain methods have been shown to enhance second order optical nonlinear susceptibility $\chi^{(2)}$ and consequently second harmonic generation. However,

these methods have limitations. With ion implantation and MBE methods alone, the strain is fixed, permanent and varies depending on which complicated fabrication protocols are employed. External strain machines produce an inhomogenous strain over a large area and cannot be incorporated directly into microelectronic or optoelectronic devices. Traditional acoustic waves produce homogenous strain and can be incorporated directly into devices. However, the speeds at which these acoustic frequencies can be generated are limited to low GHz, which makes them too slow for ultrafast processes. Frequencies obtainable with acoustic solitons are on the order of 10's of GHz to low THz. In our experimental system we can achieve acoustic waves in the frequency regime of 60-100 GHz for excitation wavelengths from 750 to 900 nm and from 345 to 450 nm. We generate ultrafast, homogenous, transient localized strain of similar magnitude of other methods, thereby enhancing electronic and optical response of any target material.

Coherent acoustic phonons (CAP) have used for material characterization in the fields of picosecond acoustics, picosecond ultrasonics, and coherent acoustic phonon spectroscopy for several decades. The process for generating coherent acoustic phonons has been verified and well understood with ultrafast pump-probe technique [26]. In our experimental setup, a laser beam is split into two beams-the pump beam and the probe beam. When the pump beam pulse strikes the sample, the transducing layer expands thermally. This expansion quickly generates an acoustic pulse tens of nanometers wide, which propagates through the sample. This acoustic pulse can have a strain amplitude up to 10^{-3}. This strain contributes to SHG enhancement. Fig. 10 shows a theoretical shape of the pump beam, which spatial size of the order of thickness of the transducing layer and a cartoon of crystal lattice modification by CAP wave. A probe beam arrives sometime later, interacting with the strain wave. The probe monitors the change in $\chi^{(2)}$ or centrosymmetry caused by a coherent acoustic wave induced by the pump beam. These waves have produced a degree of SHG enhancement in preliminary measurements. The relative arrival time at the sample between the two pulses depends on the position of the delay stage. By varying the optical delay line, one can track the optical reflectivity variation as a function of the position of the acoustic strain in the depth of the material. A portion of the probe beam reflects off of the transducing layer and another portion off of the traveling acoustic strain wave. This causes the two probe beam reflections interfering destructively or constructively, producing oscillations in the optical reflectivity. A lock-in amplifier working at the pump frequency to collects only the SHG signal generated by transient, dynamic strain (CAP pulse).

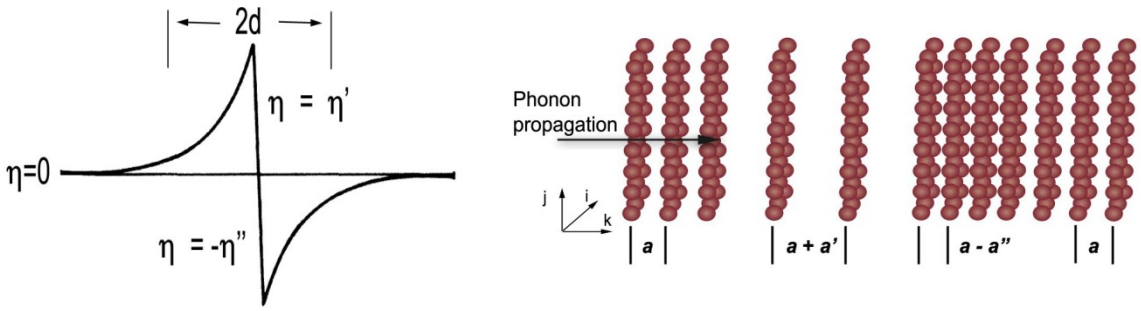

Figure 10: a) Theoretical shape of a coherent acoustic pulse, where 2d defines the spatial size of the pulse and h represents the elastic strain component [6]. b) Modification of the crystal lattice due to transient strain caused by the coherent acoustic phonon wave. The coherent pulses interact with the material and provide additional dynamic strain components to the photo-elastic tensor.

When two photons of frequency ω are destroyed and a photon of frequency 2 ω (second harmonic photon) is simultaneously emitted. The measured second harmonic intensity from the material is expressed by:

$$I_{SHG} \propto \left| P^{(2)}(2\omega) \right|^2$$

where $P^{(2)}$ is the second order nonlinear polarizability. The second order nonlinear polarizability is described by:

$$P^{(2)} = \varepsilon_0 \chi^{(2)} \boldsymbol{E}^2$$

where ε_0 is the permittivity of free space, $c^{(2)}$ is the second order nonlinear susceptibility tensor and *E* is electric field.

Experiment

The preliminary measurements were taken at room temperature on a GaAs substrate with a GaSb transducing layer. The laser is tuned to just below the band gap of GaAs to prevent carrier excitation in GaAs. The SHG spectra were observed at the following depths below the free surface: 200 nm, 400 nm, 600 nm and 800 nm. These were compared to the SHG response when there was no acoustic pulse (no pump spectrum in the Fig. 11) and also when the CAP was created at the free surface (0 ps spectrum in Fig. 11). The responses of p-polarized pump, p-polarized probe and s-polarized SHG collection (PPS) and p-polarized pump, p-polarized probe and p-polarized SHG collection (PPP) are shown in the figure below.

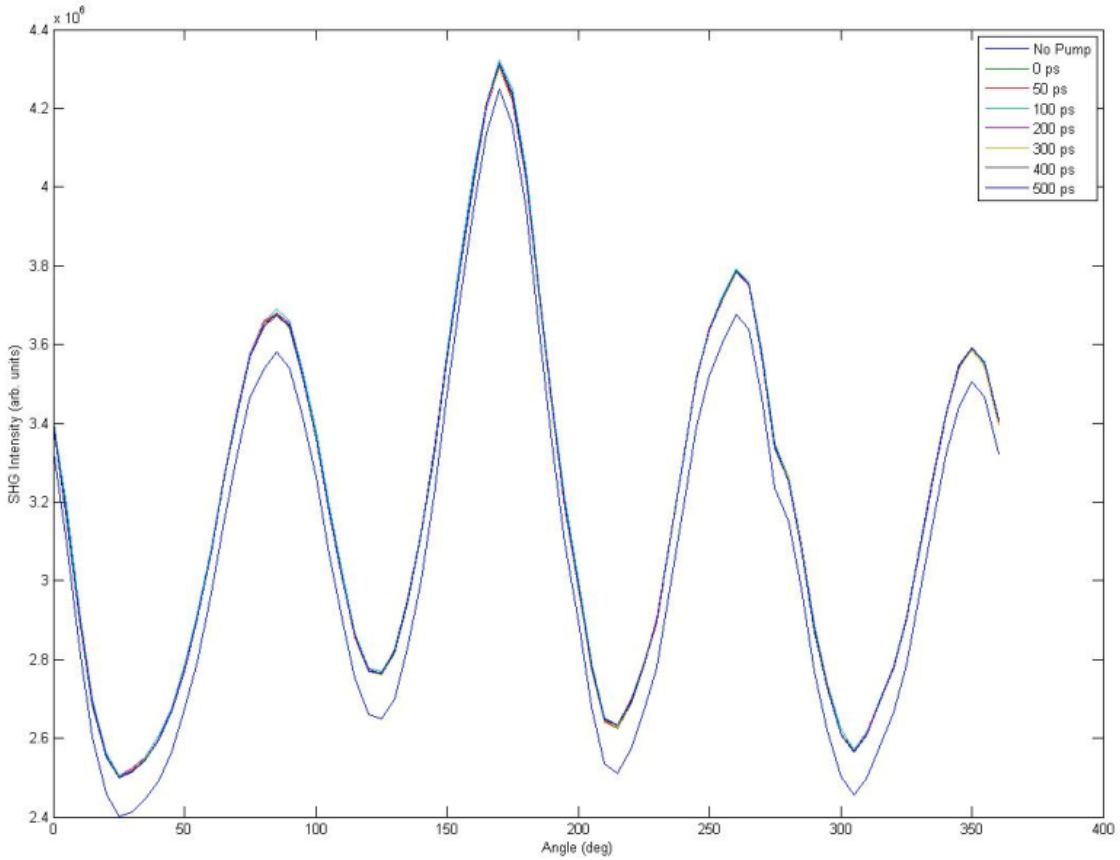

Figure 10: Four-fold symmetry containing the total SHG response from the sample at different time delays and with no pump.

The total enhancement of the SHG signal, shown in Fig. 11, is related to at least three contributions: point defects, lattice mismatch (in the case of multilayer structures) and transient strain caused by moving CAP. The areas in tension or compression (produced by CAP) change the lattice symmetry locally (see Fig. 10b). Owing to this technique we are able to measure depth-dependent SHG created only by CAP wave with accuracy of tents of nm. Figure 12 presents changes of the separated second harmonic signal produced **only** by transient ultrafast pulse, dependent on azimuth angle. That means, we are able to follow any dynamic changes in the crystal symmetry with nm resolution. Information extracted from the measurements will be verified by a phenomenological model of SHG signal and by density functional theory (DFT) calculations as well.

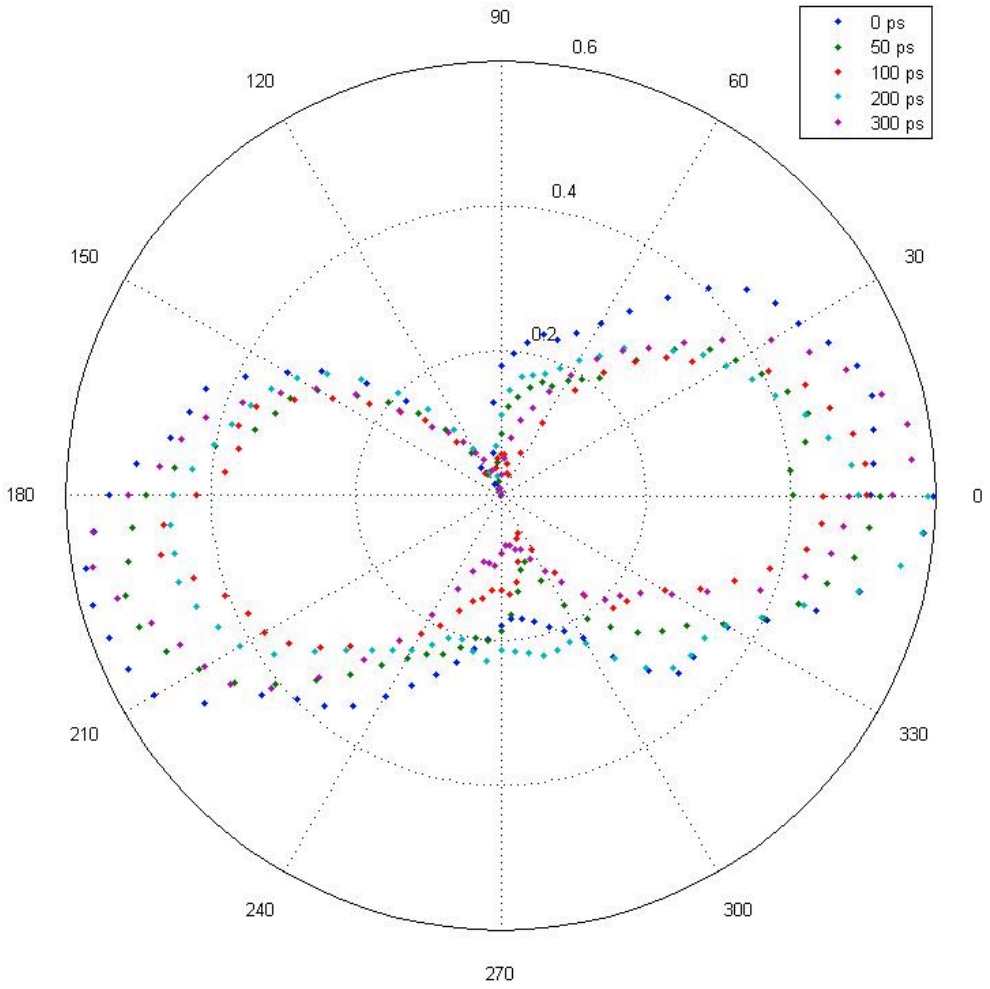

Figure 11: Two-fold symmetry SHG response containing only the second harmonic response from the CAP transient wave.

Summary

We presented work relating to two main research thrusts. The first is coherent acoustic phonon (CAP) spectroscopy of diamond crystals. We showed an ion implantation process significantly modifies the acousto-optical structure of diamond, resulting in a variety of features in the observed CAP spectra. These features were examined as a function of implantation dose and an empirical model was applied to the data, yielding good agreement. We continue this work by exploring the effects of single layer graphene on diamond with the goal of understanding how the relaxation dynamics of graphene is altered by coupling to different diamond interfaces and the effect of diamond on the scattering mechanisms involved and determining the efficiency of different pathways for energy relaxation. The second area of focus is a project assessing the transient strain produced by CAP waves. We have compared the measured CAP spectra to ab initio

calculations of the opto-electronic properties of materials. We are also using CAP waves as an active moving interface to induce local changes in electric, acoustic, and optical properties. This is able to generate ultrafast, homogenous, transient localized strains of similar magnitude of other methods, thereby enhancing electronic and optical response of any target material. We discuss the continued development of the CAP technique under the rubric of "surface physics in the bulk", specifically by applying CAP to the depth-sensitive measurement of second harmonic generation. We believe these studies will produce valuable scientific results, expand the capabilities of the CAP technique as an experimental tool, and further the goals of the ARO as laid out in the Materials by Design program.

References

1. J. K. Miller, J. Qi, Y. Xu, Y.-J. Cho, X. Liu, J. K. Furdyna, I. Perakis, T. V. Shahbazyan, and N. Tolk, "Near-bandgap wavelength dependence of long-lived traveling coherent longitudinal acoustic phonons in GaSb-GaAs heterostructures," Phys. Rev. B, vol. 74, p. 113313, Sep 2006.

2. A. Steigerwald, Y. Xu, J. Qi, J. Gregory, X. Liu, J. K. Furdyna, K. Varga, A. B. Hmelo, G. Lupke, L. C. Feldman, and N. Tolk, "Semiconductor point defect concentration profiles measured using coherent acoustic phonon waves," Appl. Phys. Lett., vol. 94, no. 11, p. 111910, 2009.

3. J. F. Ziegler, M. D. Ziegler, and J. P. Biersack, "SRIM—The stopping and range of ions in matter (2010)," Nucl. Instrum. Meth. B, vol. 268, no. 11-12, pp. 1818–1823, 2010.

4. E. O. Kane, "Band tails in semiconductors," Solid State Electron., vol. 28, no. 1–2, pp. 3–10, 1985).

5. L. Feldman, J. Mayer, and S. Picraux, Materials analysis by ion channeling: submicron crystallography. Academic Press, 1982.

6. L. C. Feldman and J. W. Rodgers, "Depth profiles of the lattice disorder resulting from ion bombardment of silicon single crystals," J. Appl. Phys., vol. 41, no. 9, pp. 3776–3782, 1970.

7. R. Kalish and S. Prawer, Ion implantation of diamond and diamond films, ch. 26, pp. 945–982. CRC Press, 1998.

8. A. Zaitsev, Optical Properties of Diamond: A Data Handbook. Springer, 2001.

9. J. Gregory, A. Steigerwald, H. Takahashi, A. Hmelo, and N. Tolk, "Ion implantation induced modification of optical properties in single-crystal diamond studied by coherent acoustic phonon spectroscopy," Appl. Phys. Lett., vol. 101, no. 18, p. 181904, 2012, 181904 (2012).

10. S. Lagomarsino, P. Olivero, S. Calusi, D. G. Monticone, L. Giuntini, M. Massi, S. Sciortino, A. Sytchkova, A. Sordini, and M. Vannoni, "Complex refractive index variation in proton-damaged diamond," Opt. Express, vol. 20, pp. 19382–19394, Aug 2012.

11. A. Battiato, F. Bosia, S. Ferrari, P. Olivero, A. Sytchkova, and E. Vittone, "Spectroscopic measurement of the refractive index of ion-implanted diamond," Opt. Lett., vol. 37, pp. 671–673, Feb 2012.

12. M. A. Draganski, E. Finkman, B. C. Gibson, B. A. Fairchild, K. Ganesan, N. Nabatova-Gabain, S. Tomljenovic-Hanic, A. D. Greentree, and S. Prawer, "Tailoring the optical constants of diamond by ion implantation," Opt. Mater. Express, vol. 2, pp. 644–649, May 2012.

13. P. Olivero, S. Calusi, L. Giuntini, S. Lagomarsino, A. L. Giudice, M. Massi, S. Sciortino, M. Vannoni, and E. Vittone, “Controlled variation of the refractive index in ion-damaged diamond,” Diam. Relat. Mater., vol. 19, no. 5-6, pp. 428–431, 2010.

14. A. V. Khomich, V. I. Kovalev, E. V. Zavedeev, R. A. Khmelnitskiy, and A. A. Gippius, “Spectroscopic ellipsometry study of buried graphitized layers in the ion-implanted diamond,” Vacuum, vol. 78, no. 2-4, pp. 583–587, 2005.

15. K. L. Bhatia, S. Fabian, S. Kalbitzer, C. Klatt, W. Krätschmer, R. Stoll, and J. F. P. Sellschop, “Optical effects in carbon-ion irradiated diamond,” Thin Solid Films, vol. 324, no. 1-2, pp. 11–18, 1998.

16. R. L. Hines, “Radiation damage of diamond by 20-keV carbon ions,” Phys. Rev., vol. 138, pp. A1747– A1751, Jun 1965.

17. Z. H. Levine, H. Zhong, S. Wei, D. C. Allan, and J. W. Wilkins, “Strained silicon: A dielectric-response calculation,” Phys. Rev. B, vol. 45, pp. 4131–4140, Feb 1992.

18. L. S. Hounsome, R. Jones, M. J. Shaw, and P. R. Briddon, “Photoelastic constants in diamond and silicon,” phys. status solidi (a), vol. 203, no. 12, pp. 3088–3093, 2006.

19. H. M. Lawler, J. J. Rehr, F. Vila, S. D. Dalosto, E. L. Shirley, and Z. H. Levine, “Optical to UV spectra and birefringence of SiO2 and TiO2: First-principles calculations with excitonic effects,” Phys. Rev. B, vol. 78, p. 205108, Nov 2008.

20. X. Gonze, J.-M. Beuken, R. Caracas, F. Detraux, M. Fuchs, G.-M. Rignanese, L. Sindic, M. Verstraete, G. Zerah, F. Jollet, M. Torrent, A. Roy, M. Mikami, P. Ghosez, J.-Y. Raty, and D. Allan, “First-principles computation of material properties: the abinit software project,” Comp. Mater. Sci., vol. 25, no. 3, pp. 478 – 492, 2002.

21. D. K. Biegelsen, “Photoelastic tensor of silicon and the volume dependence of the average gap,” Phys. Rev. Lett., vol. 32, pp. 1196–1199, May 1974.

22. T. Saka et al. Y, Strain of GaAs/GaAsP Superlattices Used as Spin-Polarized Electron Photocathodes, Determined by X-Ray Diffraction, Surf. Sci. and Nanotech. **8,** 125, 2010.

23. X. Jin et al. High-Performance Spin-Polarized Photocathodes Using a GaAs/GaAsP Strain-Compensated Superlattice, Appl. Phys. Express **6,** 015801, 2013.

24. C. Schriever et al. Strained silicon Photonics, Materials **5**, 889 2012.

25. Ji-Hong Zhao et al. Enhancement of second-harmonic generation from silicon stripes under external cylindrical strain, Opt. Lett. **34**, 3340, 2009.

26. C. Thomsen et al., Coherent Phonon Generation and Detection by Picosecond Light Pulses, Phys. Rev. Lett. 53 989, 1984.